第 6 卷　第 2 期　　航空动力学报　　Vol.6　No.2
1991 年　　4 月　　**Journal of Aerospace Power**　　Apr.　1991

离心压气机 S_1 流面流场的计算

中国科学院　　华耀南

【摘要】 本文对计算轴流压气机 S_1 流面的流函数矩阵解法的计算机程序作了修改, 使之能适合于计算离心压气机的 S_1 流面。本方法是引入人工密度, 积分运动方程求速度场, 而后求密度场, 进行迭代求解, 计算速度非常迅速。对离心压气机的几个算例表明: 只要不发生明显分离, 计算结果与实验值是符合的。本方法可用来予测离心压气机 S_1 流面流场。

一、前　　言

文献[1] 引入人工密度方法, 使弱守恒形式的流函数控制方程用统一的中心差分格式离散, 然后用矩阵直接分解求解离散后得到的代数方程组, 直接求得各网格点上的流函数值, 再积分运动方程求得速度场, 而后求得密度场, 进行迭代求解。用该方法曾计算了大量的轴流压气机的 S_1 流面上的流场, 证明本方法是非常有效的, 计算时间短, 精度高, 且能计算跨音流场。但本方法尚未计算过离心压气机。离心压气机和轴流压气机相比, 无论在结构上还是在性能上都有重大差别, 因此必须对原计算轴流压气机的程序作适当修改, 本文主要是针对离心压气机的特点, 对进、出口边界条件作了重大改进。为考验修改后的程序对离心压气机计算的适用性, 本文计算了三种离心压气机的九个 S_1 流面, 计算结果表明: 只要不发生大分离, 修改后的程序可以用来予测离心压气机 S_1 流面上的流动。

二、基本方程和计算方法

假设气体是相对稳定、绝热、无粘性的完全气体, 使用文献 [2] 中提出的非正交曲线坐标与速度分量的概念, 在离心压气机的 S_1 流面上建立非正交曲线坐标, 如图 1 所示。

由连续方程引入流函数, 代入运动方程后可得弱守恒形式的流函数方程, 无量纲化后得:

$$\frac{\partial}{\partial x^1}\left(\frac{\overline{a_{22}^*}}{\tau^*\rho^*}\left(\frac{1}{\overline{a_{11}}}\frac{\partial\psi^*}{\partial x^1}-\frac{\cos\theta_{12}}{\overline{a_{22}^*}}\frac{\partial\psi^*}{\partial x^2}\right)\right)+\frac{\partial}{\partial x^2}\left(\frac{\overline{a_{11}^*}}{\tau^*\rho^*\sin\theta_{12}}\left(\frac{1}{\overline{a_{22}^*}}\frac{\partial\psi^*}{\partial x^2}-\frac{\cos\theta_{12}}{\overline{a_{11}^*}}\frac{\partial\psi^*}{\partial x^1}\right)\right)$$

$$=2\overline{a_{11}^*}\,\overline{a_{22}^*}\Gamma\sin\sigma\sin\theta_{12}-\left(\frac{\partial\psi^*}{\partial x^2}\right)^{-1}\tau^*\rho^*\,\overline{a_{11}^*}\,\overline{a_{22}^*}\Gamma^2\sin\theta_{12}\frac{\partial s^*}{\partial x^2}\frac{a_{io}^{2\prime}}{kgU_i^2}\rho^{*\,\kappa-1}e^{(\kappa-1)s^*} \tag{1}$$

上式中 $\psi^*=\psi/G\times100$, $\rho^*=\rho/\rho_{io}'$, $\tau^*=\tau/\tau_i$, $\overline{a_{11}^*}=\overline{a_{11}}/r_i$

$$\overline{a_{22}^*}=\overline{a_{22}}/r_i,\quad s^*=s/R,\quad \Gamma=\frac{100z_n\omega r_i}{2\pi W_i\cos\beta_i}\left(1+\frac{\kappa-1}{2}Ma_i\right)^{\frac{1}{\kappa-1}}$$

ψ 为流函数, G 为质量流量, ρ 为密度, τ 为 S_1 流面流片厚度, $\overline{a_{11}}$、$\overline{a_{22}}$ 为度规系数, s 为

本文于 1990 年 2 月收到。

熵，z_n 为叶片数，ω为转速，r 为半径，W 为相对速度，β为相对气流角，Ma 为相对马赫数，下标 i 指叶栅进口处参数。引入人工密度[3]：

$$\tilde{\rho} = \rho - \mu \left[(W^1/W)\rho_{x^1}\Delta x^1 - (W^2/W)\rho_{x^2}\Delta x^2 \right] \quad (2)$$

此处 $\mu = Max\left[0, c(1 - 1/Ma^2)\right]$，$C$ 是介于 1.0～3.0 之间的常数。对全场一律采用不等距的三点中心差分格式组成的中心九点差分格式，对式 (1) 进行离散，得到：

$$A_1\Psi^*_{j-1,k-1} + A_2\Psi^*_{j,k-1} + A_3\Psi^*_{j+1,k-1} + A_4\Psi^*_{j-1,k} + A_5\Psi^*_{j,k} + A_6\Psi^*_{j+1,k} + A_7\Psi^*_{j-1,k+1} + A_8\Psi^*_{j,k+1} + A_9\Psi^*_{j+1,k+1} = D_{j,k} \quad (3)$$

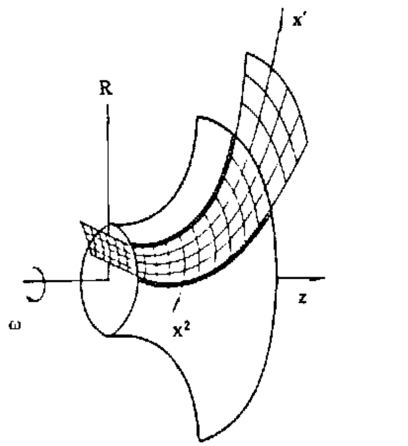

图 1　离心压气机 S_1 流面上的非正交曲线座标

上式中的A_1、A_2、A_3，……A_9 和 $D_{j,k}$是 $\overline{a^*_{11}}$、$\overline{a^*_{22}}$、θ_{12}、τ^*、ρ^* 和网格几何尺寸的函数。采用的边界条件是：进出口区边界应用周期条件；叶片表面 Ψ^* = 常数；出口边上

$$-\frac{\partial\Psi^*}{\partial x^1}\bigg\backslash\frac{\partial\Psi^*}{\partial x^2} = (\overline{a^*_{11}}/\overline{a^*_{22}})(\mathrm{tg}\beta_2\cos\theta - \sin\theta) \quad (4)$$

上式中 β_2 为出口边上气流角，θ为非正交曲线坐标x^1 和x^2 之间的夹角减去 90°(见文献 [1] 和 [2])，若x^1 方向为流线方向 (在轴流压气机中就用此假设)，则 $\beta_2 = \theta$，由 (4) 式可得：

$$\partial\Psi^* / \partial x^1 = 0 \quad (5)$$

这就是轴流压气机计算中所用的出口边上的边界条件，可见，此乃是 (4) 式的一个特例。对离心压气机 S_1 流面的实际计算表明，有时用 (5) 式表示的边界条件得不到收敛解，但用 (4) 式表示的边界条件都能得到收敛解，因此，(4) 式表示的边界条件具有更为普遍的意义。轴流压气机叶栅下游的相对气流角 β_2 基本上不变，但离心压气机，其下游的气流角随离开尾缘而迅速变化。在出口边上的气流角 β_2 与叶片角 β_{2A} 差别很大，如果仍用轴流压气机计算中的一套方法生成网格，就很不合理，网格过度斜交，导致计算失败。

进口边上的边界条件与出口边类似，可用：

$$-\frac{\partial\Psi^*}{\partial x^1}\bigg\backslash\frac{\partial\Psi^*}{\partial x^2} = (\overline{a^*_{11}}/\overline{a^*_{22}})(\mathrm{tg}\beta_1\cos\theta - \sin\theta) \quad (6)$$

在求解域中对每一个网格点列出离散的主方程 (3)，在边界点上应用上述边界条件后，我们可以得到一个线性代数方程组，写成矩阵形式：

$$[M]\{\Psi^*\} = \{p\} \quad (7)$$

上式中 $[M]$ 为系数矩阵，$\{\Psi^*\}$，$\{p\}$ 为列向量，本文采用文献 [4] 中的 $[L]$、$[u]$ 直接分解法求得全场各网格点上的 Ψ^*。另外，由运动方程可推得如下表达式：

$$\frac{\partial}{\partial x^2}\left[W^{1^*}(\overline{a^*_{11}} - \overline{a^*_{22}}\cos\theta_{12}\Psi^*_{x^1}/\Psi^*_{x^2})\right] = 右端项 \quad (8)$$

上式中的右端项是$\Psi^*_{x^1}$、$\Psi^*_{x^2}$、ρ^*……和网格几何尺寸的函数。由 (7) 式求得全场各网格点上的 Ψ^* 后，积分式 (8)，可求得全场 W^{1^*} 和 W^*，再由能量方程求得 ρ^*：

$$\rho^* = \left[(I^{*2}_i - 0.5W^{2^*} + 0.5r^{*2})/H^*_i\right]^{1/(\kappa-1)} \quad (9)$$

上式中 H 为相对总焓，$H = C_pT'_o$，$H^*_i = H_i/U^2_i$，而 $U_i = \omega r_i$。

$I^*_i = I_i/U^2_i = \left[C_pT_i + (1/2)(W^2_i - \omega^2r^2_i)\right]/U^2_i$ 为无量纲相对滞止转子焓。

三、离心压气机算例

1. 几何描述[5] A 型、B 型、C 型三种扩压程度不同的离心压气机的子午流道的几何形状描述见图 2 所示，其中 A 型的扩压程度最高，C 型最小，B 型居中。这三种压气机的导风轮的几何尺寸和结构完全一样，为一圆柱形。导风轮叶片中弧线形状为抛物线。在某一叶高处（即进口某一半径 r_1 处）圆柱面展开图（即图 3）上的坐标表达式为：

$$y = (1/2z_o)(\omega r_1/C_{1m})(z - z_o)^2 \qquad (10)$$

在本算例中，$z_o = 30\text{mm}$，且 $C_{1m} = C_{1z} = C_1$。由式 (10) 可得 $(dy/dz)_{z=0} = \omega r_1/C_{1m} = u_1/C_1 = \text{tg}\beta_1$，可见由式 (10) 规定的叶片中弧线在进口处 ($z = 0$) 切线与 z 轴夹角正好是进口处速度三角形所规定的气流角 β_1。而且不同叶高处的叶片中弧线的形状是不一样的，也就是说，导风轮叶片是扭曲的，以适应不同叶高进口处的气流角。叶片法向厚度由 $t_n = 1.5 + 1.5z/30$ 决定。其中长度单位全部为毫米。叶轮叶片由 12 个径向直叶片组成，叶片厚度不变为 $3mm$。

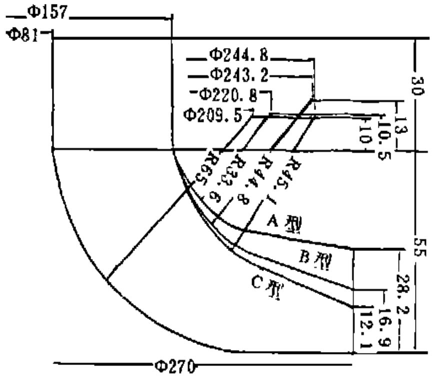

图 2 三种离心压气机的子午流道

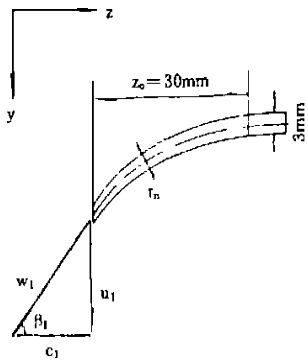

图 3 导风轮叶片中弧线

2. 实验操作条件[5,6] 测点布置如图 4 所示。实验条件是：压气机转速 $\omega = 628.3\text{rad/s}$，流量系数 $\Phi = C_{2r}/u_2 = 0.5$，进出口子午速度比 $D_m = C_{2m}/C_{1m}$ 对 A、B、C 三种类型的压气机分别为 0.6、1.0 和 1.4。

3. 计算结果 每种类型压气机算了三个 S_1 回转流面。其形状与文献 [4] 中给定的测点一致（见图 4）。它们是把子午流道在几何上分成 8 等分。

(1) A 型压气机的 1/8、4/8、7/8 三个 S_1 回转流面的计算结果表示在图 5 中。对 A 型压气机而言计算与测量值相差较大，根据文献 [7] 的实测结果，对 A 型压气机在离进口 30%（$l/l_t = 0.3$）时就发生分离，本文的无粘计算方法的结果不能反应这种分离流动，故相差较大。图中还画出了文献 [6] 的全三元无粘计算结果，与实验结果也相差较大。

(2) B 型与 C 型压气机的 1/8、4/8、7/8 的三个 S_1 回转流面的计算结果示于图 6。计算和测量值比较符合。因为据文献 [7] 的实测，B 型压气机内没有发生大的分离（图 6 之 a、b、c）。

由于 C 型压气机也没有发生大的分离流动，所以计算值与实验值也符合得较好（图 6 之 d、e、f）。

4. 滑移系数的计算结果 对径向式叶轮，滑移

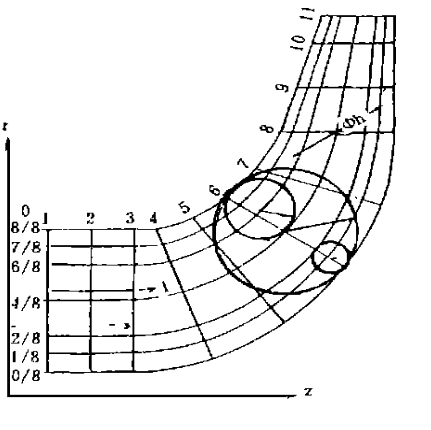

图 4 S_1 回转流面的母线和测点布置

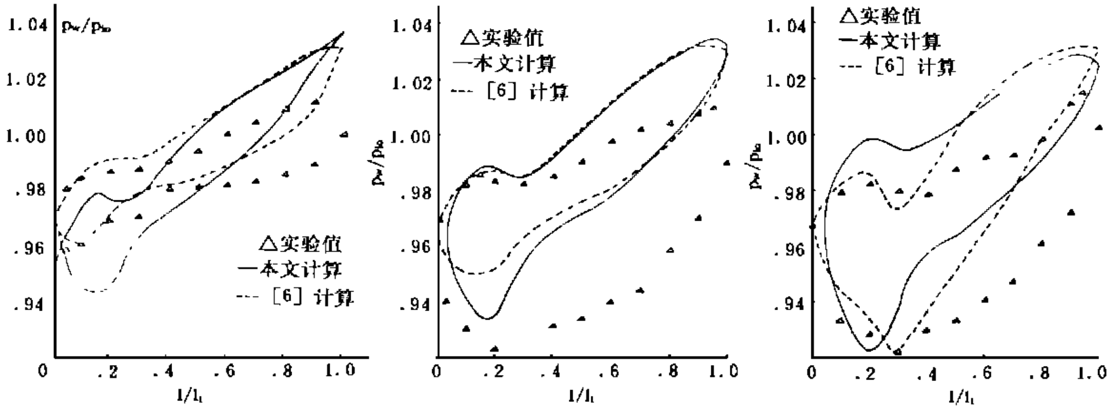

图 5 叶片表面静压分布 (*A* 型)

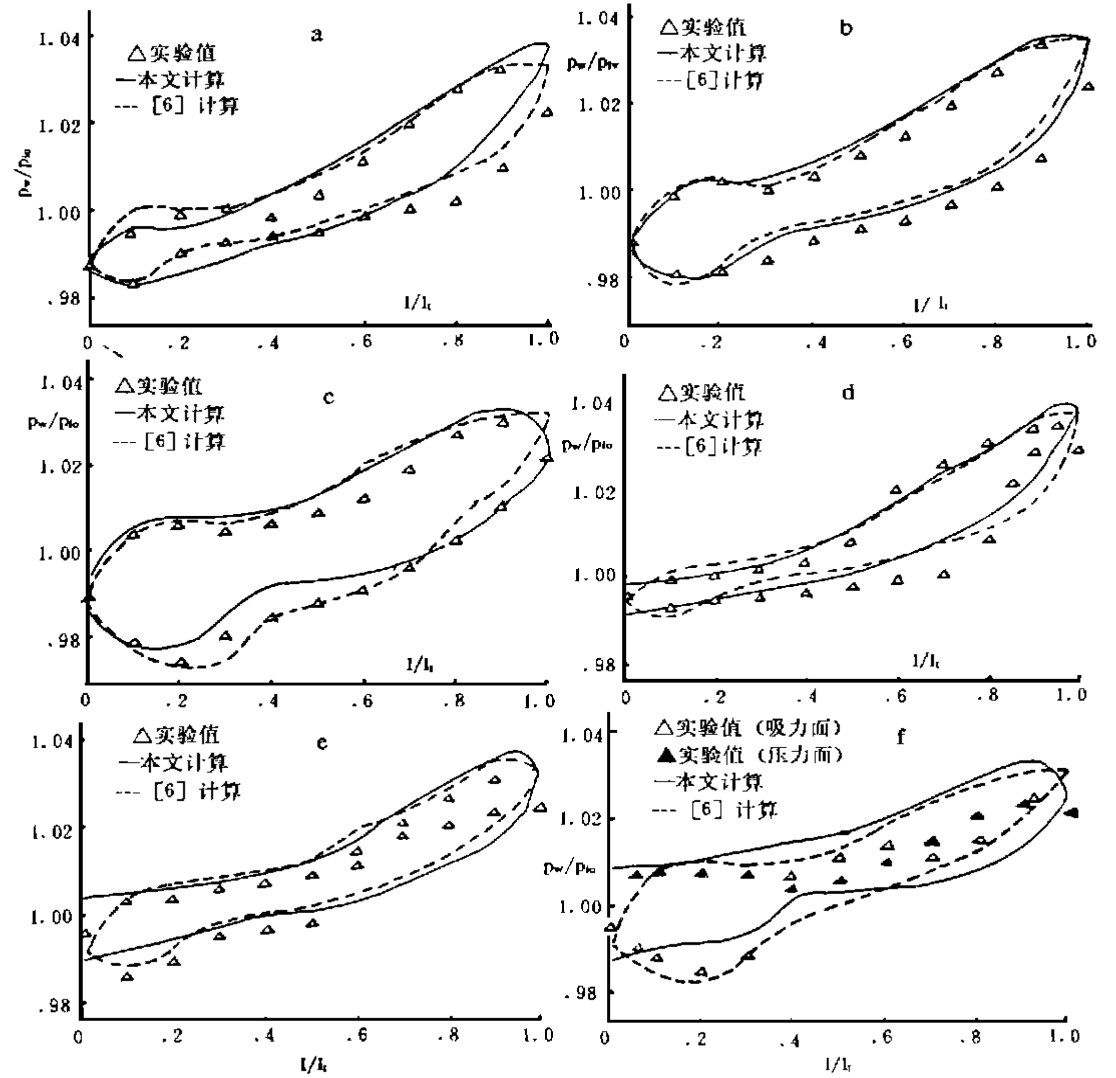

图6 叶片表面静压分布 (*B* 型: *a*、*b*、*c*; *C* 型: *d*、*e*、*f*)

系数的定义是 $\mu = C_{2u}/u_2$，许多文献常用下列公式计算[8,9]

$$\mu = 1/\left\{1 + (2/3)(\pi/z_n)\left(1\Big\backslash\left(1 - r_m^2/r_2^2\right)\right)\right\} \quad (11)$$

上式中 $r_m = \sqrt{(1/2)(r_{1h}^2 + r_{1t}^2)}$，$r_{1h}$、$r_{1t}$分别是导风轮进口内、外径。

本文得到的流场计算结果满足连续方程和考虑旋转的运动方程和能量方程，因此，气体在有限叶片内的流动会出现的与叶轮旋转方向相反的轴向旋涡也已经计及在内。由本文流场计算得到的叶轮出口处中心流线上的 C_{2u} 按滑移系数的定义计算得到的 μ，和按公式 (11) 计算得到的 μ 的对比列于表 1。A 型压气机未列入在内 (因存在大分离)。

表 1 μ 的对比

压气机类型	B 型			C 型		
S_1 流面	1/8	4/8	7/8	1/8	4/8	7/8
本文计算 μ	.8901	.8783	.8441	.8123	.8217	.8359
公式 (11) 计算 μ	.8183			.8183		

本文的计算结果是仅用一次 S_1 流面计算得出的结果，没有进行 S_1/S_2 两类流面迭代。尽管如此，得出的叶片表面静压分布的计算结果也比较符合实验值。文献 [6] 是用 S_1/S_2 两类流面迭代得到的全三元计算结果，趋势与本文得到的结果完全一致 (见图 5、6)。因此，本文所应用的方法是相当精确的。计算方法也迅速，以上每一个算例，只需迭代 6～8 次，$\left|\rho^{*(n+1)} - \rho^{*(n)}\right| < 10^{-5}$，$\left|\psi^{*(n+1)} - \psi^{*(n)}\right| < 10^{-4}$。每一个算例只需 2～3 分钟 (UNUVAC 1100 计算机)，因此本文方法适用于工程计算。

参 考 文 献

[1] 华耀南、吴文权，"S_1 流面跨声速流场流函数矩阵解"，工程热物理学报，Vol. 8，No. 2，1987 年。

[2] 吴仲华，"使用非正交曲线坐标和非正交速度分量的叶轮机械三元流动基本方程及其解法"，机械工程学报，1979 年第 1 期。

[3] Hafez, M., "Artificial Compressibility Method for Numerical Solution of Transonic Full Potential Equation", AIAA Journal, Vol. 17, No. 8, 1979.

[4] 吴文权、刘翠娥，"使用非正交曲线坐标和非正交速度分量的 S_1 流面正问题流场矩阵解"，工程热物理学报，Vol. 1，No. 1，1980 年。

[5] Mizuki, S., "Description of Compressor Geometries", Presented at the 25th Aunual International Gas Turbine Conference and Exhibit and the 22nd Annual Fluids Engineering Conference, New Onleans, Louisiana, March 9-13, 1980.

[6] Adder D., "Comparision between the Calculated Subsonic Inviscid 3D Flow in a Centrifugal Impellar and Measurements", Presented at the 25th Annual Internatinal Gas Turbine Conference Exhibit and the 22nd Annual Fluid Fugineering Conference, New Orleaus, Louisiana, March 9-13, 1980.

[7] Mizuki S., et al, "Investigation Concerning the Blade Loading of Centrifugal Impellers", ASME Paper No. 74-GT-143, 1974.

DEVELOPMENT OF ENGINE FAULT EQUATIONS

Fan Zuomin, Sun Chunlin, Lin Zhaofu, Gao Haichuan
(*Civil Aviation Institute of China*)

ABSTRACT The engine diagnosis problem lies in solution of the engine fault equations which express the relationships between the measurements and a large set of possible but improbable mulfunctions. The engine fault equations are generally underdetermined and can be solved by the aid of Main Characteristic Parameter Model (MCPM) suggested by the authors. The engine fault equations are based on engine fault samples and can be called empirical fault equations. The empirical fault equations are similar to fault equations obtained by single factor experiments, but the engine fault samples are used instead of the results of special experiments. Differing from the small change equation, the empirical fault equations are easily obtained and are of great use for diagnosis of such faults which are difficult to be diagnosed by employing small change equations. Some practical examples of engine fault diagnosis are also given. The fault diagnosis results obtained from are very satisfactory.

FINITE ANALYTIC SOLUTION OF TURBULENT FLOW FIELD THROUGH CASCADE OF AIRFOIL

Xu Diao and Wu Guochuan (*Nanjing Aeronautical Institute*)

ABSTRACT The finite analytic method is used in the present study to calculate the turbulent flow field described with Navier-Stokes equations in body-fitted curvilinear coordinate system. The finite analytic method invokes the analytic solution of governing partial differential equations in formulating the algebraic equations that relates a nodal value in an element to its neighbouring nodal values. The major feature of the finite analytic method is its ability to simulate automatically the upwind influence of neighbouring nodal values according to direction and magnitude of convection. It is shown that the finite analytic method has good numerical stability and accuracy. The turbulent flow fields through a two-dimensional channel and a cascade of airfoil are numerically simulated by using finite analytic method in the present study. The k-ϵ turbulence model and wall function method are also employed. The agreement of numerical solution with experimental data is quite good.

FLOWFIELD MATRIX SOLUTION ON S_1 STREAMSURFACE IN A CENTRIFUGAL COMPRESSOR

Hua Yaonan (*Academia Energetics R&D Center*)

ABSTRACT The existing flowfield matrix solution method on S_1 stream surface for the calculation of flowfield in an axial compressor is extended to calculation of flowfield in a centrifugal compressor. The stream function governing equation of fluid flow has been established with respect to non-orthogonal curvilinear coordinates. By the aid of artificial compressibility method, the discretzation of the partial differential equation is accomplished with the standard central difference formula. The set of linear algebraic equations obtained is solved by means of the direct matrix method. The velocities at grid nodes are first determined by integrating the momentum equation and then the densities are obtained from the energy equation. Nine numerical examples of three types of the centrifugal compressors show that the solution obtained by the present method is in good agreement with experimental data, provided that there is no large flow separation in compressors.

PREDICTION OF LONG BLADE FLUTTER IN A STEAM TURBINE

Tao Deping, Yang Xiaodong, Zhou Shen

(***Beijing University of Aeronautics and Astronautics***)

ABSTRACT The flow characteristics of the last stage of the steam turbine are analysed on the basis of the results obtained from the cascade experiments and flow field calculation. In the case of low volumetric flow rate, the large scale separation occurs in the last stage rotor hub, and the height of separated flow region increases as the volumetric flow rate decreases. Flow separation appears at the blade pressure surface as the bulk flow enters the rotor with large negative incidence. The flow in the rotor can be divided into three regions —— a separated hub flow region, an attached-flow region and a separated-flow region. The dimensions of the three regions vary with the flow rate. The flow pattern in the last stage is very complicated. Aseries of deforming actuator disk methods and a numerical method have been developed to predict the blade flutter. The deforming actuator disk method system is applicable to calcalating 2-D and 3-D unsteady flow fields and also to calculating the bending mode and the torsional mode blade flutters. The analytical and numerical deforming actuator disk methods for predicting the blade flutter in a compressor or a steam turbine have been developed in consideration of variability of or invariabiity of the interblade phase angle. The small-disterbance potential amplitude equation is adopted in the numeried method for unsteady flow in the cascade, while the airfoil thickness and bending degree are arbitrary and the rotating finite difference scheme is employed in the calculaton of transonic flow field. The comparison between the computational and the experimental results shows that the presented methods are feasible in prediction of the flutter in blade design.

NUMERICAL SIMULATION OF TRANSITIONAL FLOWS OVER A FLAT PLATE

Jiang Hongde (***Institute of Engineering Thermophysics***)

J. G. Moore and J. Moore (***Virginia Polytechnic Institute and State University***)

ABSTRACT A new version of one-equation turbulence model for predicting the incompressible, transitional flow over a flat plate is developed. Based on an analysis of the existing one-equation models and some physical features of the transitional flow, both the eddy viscosity and turbulence length scale in the turbulence kinetic energy equation are modified in order to bring the low Reynolds number effect into the new model. The capability of this model for predicting the transitional flow is demonstrated by an extensive numerical testing for flat plate flow under free stream turbulence intensity ranging from 0.03 to 8 percent. Both the start and length of the transition are correctly predicted. Comparison of the calcutated results of both the mean and fluctuating flow properties with experimental data indicates the agreement between them is very good. A time-averaged picture for a complete boundary flow from purely